is an average of at least three measurements. The experimental uncertainties in $K_{o/w}$ and C_s^w are around 1.0%. An asterisk is used to indicate that the literature data are calculated values according to Hansch, Quinlan, and Lawrence (*4*). Our results are generally in good agreement with available experimental literature data.

The present data were subjected to a linear regression of log $K_{o/w} = c \log \gamma_s^w + d$ for each class of compound and for all compounds taken together. The results of these analyses are shown in Table VIII.

According to eq 5, the slope for each class should be unity and the negative of the intercept is log γ_s^o (assumed to be relatively constant). Examination of Table VIII shows that the slopes are indeed close to unity, ranging between 0.91 and 1.08. The small deviations are most likely caused by slight variations in log γ_s^o within each class (*11*). For example, the average of the difference between log γ_s^w and log $K_{o/w}$ for the aromatic compounds of Table I is 0.56 and for halogenated hydrocarbons of Table III is 0.68, whereas their least-squares values listed in Table VIII for the intercepts are respectively -0.77 and -0.32. Therefore, the intercepts represent only approximate (averaged) values of log γ_s^o for each class.

These findings show that the octanol/water partition coefficient of a solute may be estimated with reasonable accuracy from knowledge of its aqueous solubility, its molar volume, and the regression equation for compounds of its class. Also, this study establishes that the generator column method coupled with either HPLC or GC modes of analysis provides an accurate and rapid method for systematic determination of $K_{o/w}$ and C_s^w for organic compounds.

Literature Cited

(1) Hansch, C.; Dunn, W. J. *J. Pharm. Sci.* **1972**, *61*, 1.
(2) Lyman, W. J. In "Handbook of Chemical Property Estimation Methods; Environmental Behavior of Organic Compounds"; Lyman, W. J., Reehl, W. F., Rosenblatt, D. H., Eds.; McGraw-Hill: New York, in press.
(3) Hansch, C.; Leo, A. "Substituent Constants for Correlation Analysis in Chemistry and Biology"; Wiley-Interscience: New York, 1979.
(4) Hansch, C.; Quinlan, J. E.; Lawrence, G. L. *J. Org. Chem.* **1968**, *33*, 347.
(5) MacKay, D.; Bobra, A.; Shiu, W. Y.; Yalkowsky, S. M. *Chemosphere* **1980**, *9*, 701.
(6) DeVoe, H.; Miller, M. M.; Wasik, S. P. *J. Res. Natl. Bur. Stand.* **1981**, *86*, 361.
(7) May, W. E.; Wasik, S. P.; Freeman, D. M. *Anal. Chem.* **1978**, *50*, 997.
(8) McAuliffe, C. *J. Phys. Chem.* **1966**, *70*, 1267.
(9) Reddick, J.; Burger, W. "Techniques of Organic Chemistry"; Wiessburger, A., Ed.; Wiley-Interscience: New York, 1955; Vol. 2.
(10) Sutton, C.; Calder, J. A. *J. Chem. Eng. Data* **1975**, *20*, 320.
(11) Tewari, Y. B.; Miller, M. M.; Wasik, S. P. *J. Res. Natl. Bur. Stand. (U.S.)*, in press.
(12) Certain trade names and company products are identified in order to adequately specify the experimental procedure. In no case does such identification imply recommendation or endorsement by the National Bureau of Standards, or does it imply that the products are necessarily the best available for the purpose.

Received for review October 28, 1981. Accepted April 5, 1982. We gratefully acknowledge the financial support of the Environmental Protection Agency and the Toxic Control Act.

Isopiestic Determination of the Activity Coefficients of Some Aqueous Rare-Earth Electrolyte Solutions at 25 °C. 6. $Eu(NO_3)_3$, $Y(NO_3)_3$, and YCl_3

Joseph A. Rard*

University of California, Lawrence Livermore National Laboratory, Livermore, California 94550

Frank H. Spedding

Ames Laboratory, U.S. Department of Energy, and Department of Chemistry, Iowa State University, Ames, Iowa 50011

The osmotic coefficients of aqueous $Eu(NO_3)_3$, $Y(NO_3)_3$, and YCl_3 have been measured at 25 °C from dilute solution to supersaturated concentrations with the isopiestic method. Least-squares equations were fitted to these osmotic coefficients, which were then used to calculate water activities and mean molal activity coefficients. Pitzer's equations were also fitted to the lower-concentration data. These results are compared to published activity data for rare-earth chlorides, perchlorates, and nitrates. A total of 40 rare-earth salts have now been studied, and their activities are discussed in terms of cation hydration and anion–cation interactions. Density data are also reported for $Y(NO_3)_3$ solutions.

Introduction

In the late 1940s activity coefficient measurements began at Ames Laboratory for dilute rare-earth halide solutions at 25 °C, using emf measurements. Data were ultimately published for 14 rare-earth chlorides and 9 rare-earth bromides (*1*, *2*). In the 1950s isopiestic measurements were started for rare-earth electrolyte solutions at higher concentrations. This research was moved to Lawrence Livermore National Laboratory (LLNL) in 1977. Isopiestic data have already been published for 14 rare-earth chlorides, 12 perchlorates, and 12 nitrates at 25 °C (*3*-*7*).

Activity data for aqueous rare-earth salts are interesting for several reasons. The weakly complexed chlorides, bromides, and perchlorates show S-shaped series trends at constant molality, which are mainly due to total hydration trends for the cations. These trends are strongly influenced by an inner-sphere hydration number decrease between Nd^{3+} and Tb^{3+} and its concomitant contraction of the inner-sphere hydrated radius (*8*, *9*). In contrast, rare-earth nitrate solutions contain mixtures of inner- and outer-sphere complexes which cause these S-shaped series trends to disappear at fairly low concentrations (*7*).

A so-called gadolinium break appears in many properties of rare-earth complexes, but it is conspicuously absent for most thermodynamic (*3*, *4*, *10*, *11*) and transport properties (*12*, *13*) of rare-earth chlorides and perchlorates. However, most properties of rare-earth nitrates have a "bulge" in the middle

0021-9568/82/1727-0454$01.25/0

Table I. Isopiestic Molalities of Some Rare-Earth Electrolyte Solutions from Measurements with KCl Reference Solutions

$[Eu(NO_3)_3]$, m	$[Y(NO_3)_3]$, m	$[YCl_3]$, m	[KCl], m	Φ(KCl)
0.148 93	0.140 38	0.138 66	0.24267	0.9091
0.234 05	0.218 47	0.214 21	0.38777	0.9021
0.244 30	0.228 14	0.223 33	0.40559	0.9015
0.272 79	0.253 94	0.248 01	0.45452	0.9002
0.497 59	0.455 87	0.434 38	0.87928	0.8969
0.531 57	0.485 79	0.462 08	0.94933	0.8971
0.539 31	0.492 83	0.468 60	0.96439	0.8971
0.606 15	0.552 08	0.521 04	1.1021	0.8980
0.678 37	0.616 48	0.577 79	1.2562	0.8995
0.762 27	0.691 08	0.642 19	1.4408	0.9018
0.842 07	0.761 74	0.702 29	1.6232	0.9045
0.930 47	0.840 39	0.767 67	1.8288	0.9080
1.018 3		0.831 46	2.0394	0.9121
1.037 2		0.844 45	2.0840	0.9130
1.043 3	0.940 97	0.849 68	2.1025	0.9134
1.061 5		0.863 30	2.1447	0.9143
1.166 0	1.051 7	0.938 27	2.4117	0.9203
1.188 8	1.070 8	0.953 48	2.4693	0.9216

of the series at high concentrations. Activity data were lacking for $Eu(NO_3)_3$, so it was not known whether this "break" appears at Gd^{3+} or some other rare earth. Activity data are now reported for $Eu(NO_3)_3$ and confirm that a gadolinium break is present for rare-earth nitrates.

Yttrium is classified as a rare earth because it forms a trivalent ion and because its ionic radius falls within the range for lanthanides, even though it contains no 4f electrons. However, its position in the rare-earth series is known to vary with the anion and with the property beging investigated. Therefore, isopiestic and density measurements were performed for $Y(NO_3)_3$ to determine its position within the nitrate series. Previous activity data for YCl_3 were of lower accuracy than for other rare-earth chlorides at high concentrations (*3*), so its osmotic coefficients were remeasured.

Experimental Section

The experimental details are nearly identical with those for the previous two studies (*6*, *7*). All equilibrations were performed at 25.00 ± 0.005 °C (IPTS-68). Isopiestic equilibration times ranged from 4 to 41 days, with the longer times required at lower concentrations. The saturated-solution concentration of YCl_3 (solid phase presumably $YCl_3 \cdot 6H_2O$) was determined to be 3.9367 ± 0.0035 mol/kg by using 9- and 10-day isopiestic equilibrations.

$CaCl_2$ stock no. 1 and KCl were used as isopiestic standards. They have already been described (*14*). The molecular masses used were 337.975 g/mol for $Eu(NO_3)_3$, 274.921 g/mol for $Y(NO_3)_3$, 195.265 g/mol for YCl_3, 110.986 g/mol for $CaCl_2$, and 74.551 g/mol for KCl.

Rare-earth electrolyte solutions were prepared from pure rare-earth oxides and analytical reagent grade HNO_3 or HCl. The stock solutions were adjusted to their equivalence concentrations with dilute solutions of their corresponding acids. These equivalence concentrations were determined by pH titration of samples with dilute acid solutions. Each rare-earth solution pH at the end of the titration curve was about 1 pH unit below that of the acid used for the titration. This indicates that hydrogen ion activities in rare-earth electrolyte solutions are much larger than their concentrations (hydrogen ion activity coefficients > 1).

The Y_2O_3 sample used for preparation of stock solutions had been purified at Ames Laboratory by ion-exchange methods. Mass-spectroscopic analysis at Ames Laboratory indicated that the Y_2O_3 contained (in atomic percent) 0.0024% other rare earths, 0.046% Ca, 0.002% Fe, and 0.0023% of other elements.

The Eu_2O_3 was high-purity commercial material, and it was analyzed for impurities at LLNL. Direct current arc optical emission spectroscopy indicated (in weight percent) 0.06% Gd, <0.001% Cu, 0.0005% each of B and Fe, 0.0004% Mg, and <0.001% Si. X-ray fluorescence spectroscopy detected 0.04% Gd and 0.006% Dy by weight. No other impurities were found.

Stock-solution concentrations were determined by conversion of samples to the anhydrous sulfates at 500 °C. The precision of each analysis was 0.02–0.03%, and replicate sulfate analyses for $Eu(NO_3)_3$ and YCl_3 also agreed within this limit. However, mass titration of YCl_3 with $AgNO_3$ gave a concentration about 0.1% higher than sulfate analyses. This suggests that the accuracy of each analysis is only 0.05–0.1%.

Before sulfate analyses of rare-earth nitrate solutions, the nitrate ions were decomposed by evaporation with HCl. This was necessary to avoid coprecipitation of nitrate ions, which would give high results for the apparent concentrations (*5*). Rare-earth sulfate samples, prepared in this manner, were "nitrate free" as determined by the sensitive chromotropic acid test (*15*).

Published differential thermal analysis results (*16*) indicate that it should be possible to thermally decompose rare-earth nitrates to form the pure oxides. However, a sample of $Y(NO_3)_3$ that was heated overnight at 770 °C gave a distinct positive test for nitrate ions (*15*). In addition, semiquantitative tests with $Eu(NO_3)_3$ and $Y(NO_3)_3$ indicated that weighing samples as the oxides could give concentration errors of as much as 1% at 1 mol/kg, and 3% at very high concentrations. For these tests $Eu(NO_3)_3$ was heated several days at 770 °C and $Y(NO_3)_3$ at 650 °C; these temperatures are above their minimum oxide formation temperatures (*16*). Direct pyrolysis of rare-earth nitrates to the oxides is therefore unsatisfactory as a quantitative method of analysis.

Duplicate samples were used for each solution in the isopiestic equilibrations. The average equilibrium molalities are known to ±0.1% or better, with most equilibrations precise to ±0.05%. These isopiestic equilibration molalities are reported in Tables I and II.

The highest-concentration equilibrations were for supersaturated concentrations. YCl_3 showed only a slight tendency to supersaturate under isothermal conditions, whereas the nitrate solutions were stable to high degrees of supersaturation. On the basis of data for other rare-earth nitrates (*5*), we estimate that the 25 °C solubility of $Eu(NO_3)_3$ is 4.33 ± 0.03 mol/kg and that of $Y(NO_3)_3$ is 5.6 ± 0.8 mol/kg. Sample cups were examined for crystals after each high-concentration equilibration. None were present for rare-earth nitrates; this indicates that the crystallization limits had not been reached. Crystallization occurred for YCl_3 when measurements were attempted at higher concentrations.

All weights were converted to vacuum by using the appropriate densities. Published density data were available for all of the solutions except $Eu(NO_3)_3$ and $Y(NO_3)_3$. The averages of $Sm(NO_3)_3$ and $Gd(NO_3)_3$ densities (*17*) were used for the $Eu(NO_3)_3$ buoyancy corrections. Densities of $Y(NO_3)_3$ solutions were measured in duplicate, with an accuracy of 3×10^{-5} g/cm^3, by using a matched pair of single-stem pycnometers. These densities are listed in Table III.

Calculations

The $Y(NO_3)_3$ density data of Table III were represented by least-squares equations

$$d = d^0 + \sum_{i=2}^{n} B_i X^{i/2} \qquad (1)$$

where $X = m$ in mol/kg or c in mol/dm^3. The density of pure water, d^0, was set at 0.997 045 g/cm^3 (*18*). Least-squares

Table II. Isopiestic Molalities of Some Rare-Earth Electrolyte Solutions from Measurements with $CaCl_2$ Reference Solutions

$[Eu(NO_3)_3]$, m	$[Y(NO_3)_3]$, m	$[YCl_3]$, m	$[CaCl_2]$, m	$\Phi(CaCl_2)$	$[Eu(NO_3)_3]$, m	$[Y(NO_3)_3]$, m	$[YCl_3]$, m	$[CaCl_2]$, m	$\Phi(CaCl_2)$
1.0995	0.99105	0.89063	1.2310	1.1117	5.1309	4.7530	3.3303	4.9704	2.5631
1.1851	1.0685	0.95159	1.3240	1.1410	5.2528	4.8677	3.4001	5.0735	2.6006
1.2795	1.1535	1.0185	1.4264	1.1743	5.3052	4.9159	3.4282	5.1135	2.6149
1.3875	1.2504	1.0922	1.5396	1.2121		4.9846	3.4693	5.1779	2.6376
1.5079	1.3601	1.1748	1.6689	1.2565	5.3823			5.1800	2.6384
1.6280	1.4689	1.2551	1.7918	1.2999	5.4299	5.0322	3.4992	5.2212	2.6528
1.7260	1.5589	1.3202	1.8936	1.3366	5.5241	5.1241	3.5539	5.3032	2.6809
1.8665	1.6880	1.4113	2.0373	1.3895		5.1561	3.5723	5.3314	2.6904
1.9742	1.7876	1.4816	2.1462	1.4303	5.6158			5.3791	2.7064
2.0768	1.8821	1.5460	2.2486	1.4693	5.7336			5.4759	2.7380
2.1801	1.9788	1.6125	2.3523	1.5093		5.3707	3.6988	5.5235	2.7532
2.3095	2.0996	1.6939	2.4796	1.5590			3.7240	5.5660	2.7666
2.4005	2.1851	1.7490	2.5685	1.5940	5.8756			5.5956	2.7757
2.5185	2.2951	1.8225	2.6809	1.6388		5.4782	3.7638	5.6252	2.7848
2.6132	2.3821	1.8791	2.7721	1.6753			3.8086	5.6994	2.8072
2.7168	2.4811	1.9416	2.8697	1.7148	6.0203			5.7208	2.8135
2.8199	2.5765	2.0035	2.9660	1.7539		5.6246		5.7556	2.8236
2.9136	2.6664	2.0606	3.0528	1.7893	6.1351			5.8234	2.8430
3.0206	2.7658	2.1235	3.1504	1.8294			3.9138	5.8654	2.8547
3.1354	2.8744	2.1892	3.2565	1.8731			3.9191	5.8761	2.8577
3.2600	2.9942	2.2642	3.3706	1.9202		5.7684		5.8977	2.8636
3.3564	3.0846	2.3195	3.4542	1.9548			3.9367[a]	5.9006	2.8644
3.4740	3.1941	2.3868	3.5588	1.9982		5.7936		5.9193	2.8694
3.5955	3.3109	2.4598	3.6669	2.0430	6.3163			5.9823	2.8861
3.6526	3.3633	2.4904	3.7159	2.0633		5.9038	4.0101	6.0236	2.8968
3.8451	3.5440	2.6035	3.8837	2.1327	6.3858			6.0465	2.9026
3.8825	3.5767		3.9170	2.1465		6.0333	4.0843	6.1487	2.9278
4.0282	3.7124	2.7043	4.0378	2.1962		6.0517		6.1622	2.9310
4.0401	3.7251	2.7125	4.0482	2.2005		6.1151		6.2285	2.9464
4.0625	3.7530	2.7243	4.0695	2.2092		6.2855		6.3929	2.9820
4.1882	3.8692	2.7998	4.1821	2.2552		6.3107		6.4185	2.9872
4.2899	3.9617	2.8560	4.2664	2.2894		6.3751		6.4851	3.0004
4.3877	4.0591	2.9137	4.3532	2.3244		6.6554		6.7701	3.0496
4.5697	4.2264	3.0172	4.5061	2.3854		6.7550		6.8847	3.0664
4.6482	4.3037	3.0633	4.5727	2.4116		6.8023		6.9313	3.0727
4.7542	4.4011	3.1209	4.6590	2.4453		7.0171		7.1631	3.1002
4.8755	4.5151	3.1885	4.7576	2.4832		7.1073		7.2643	3.1103
5.0068	4.6371	3.2624	4.8683	2.5251		7.2103		7.3950	3.1218

[a] Saturated solution.

Table III. Densities and Apparent Molal Volumes of Aqueous $Y(NO_3)_3$ at 25 °C

m, mol/kg	c, mol/dm³	d, g/cm³	ϕ_v, cm³/mol
0.052353	0.052062	1.008 76	50.030
0.094246	0.093518	1.017 98	51.200
0.16775	0.16580	1.033 97	52.344
0.26243	0.25805	1.054 23	53.481
0.37821	0.36948	1.078 51	54.607
0.51597	0.50013	1.106 80	55.640
0.67525	0.64845	1.138 59	56.809
0.85658	0.81367	1.173 61	58.100
1.0579	0.99263	1.211 21	59.338
1.3274	1.2246	1.259 21	61.018
1.5962	1.4474	1.304 66	62.573
1.8729	1.6676	1.348 87	64.136
2.1477	1.8774	1.390 29	65.653
2.5904	2.1974	1.452 43	67.889
3.0261	2.4913	1.508 19	69.956
3.4920	2.7842	1.562 74	71.953
3.9486	3.0509	1.611 40	73.770
4.4130	3.3034	1.656 72	75.448
4.4130	3.3034	1.656 74	75.443
5.1124	3.6503	1.717 57	77.763
5.9744	4.0304	1.782 67	80.236

coefficients for eq 1 are reported in Table IV. Six coefficients were required for the molarity fit, which had a standard deviation $\sigma = 2.8 \times 10^{-5}$ and a maximum deviation of 4.2×10^{-5} g/cm³. In contrast, the molality fit required eight terms for comparable accuracy, with $\sigma = 3.2 \times 10^{-5}$ and a maximum deviation of 4.8×10^{-5}.

Apparent molal volumes of $Y(NO_3)_3$ are also reported in Table III. They were calculated with the equation

Table IV. Coefficients for $Y(NO_3)_3$ Density Polynomials

B_i	molality	molarity
B_2	0.224 885 3	0.229 763 4
B_3	0.004 116 77	−0.026 277 82
B_4	−0.063 276 42	0.032 196 42
B_5	0.090 279 39	−0.028 874 09
B_6	−0.085 830 67	0.010 284 08
B_7	0.042 961 58	−0.001 388 38
B_8	−0.010 694 25	0.0
B_9	0.001 059 433	0.0

Table V. Coefficients and Powers for Osmotic Coefficient Polynomials

i	r_i	$A_i(Eu(NO_3)_3)$	r_i	$A_i(Y(NO_3)_3)$	r_i	$A_i(YCl_3)$
1	0.75	−8.533 292	0.75	−2.993 748	1.00	39.84457
2	0.875	41.385 88	1.00	45.225 02	1.25	−150.4004
3	1.00	−35.820 81	1.25	−110.684 9	1.50	304.4071
4	1.50	8.533 200	1.50	131.794 7	1.75	−372.9891
5	2.00	−5.007 543	1.75	−85.101 86	2.00	272.48852
6	2.25	2.664 265	2.00	28.622 32	2.25	−107.9952
7	2.50	−0.431 411	2.25	−3.941 397	2.50	17.74698
σ		0.001 3		0.001 6		0.0017

$$\phi_v = \frac{10^3(d^0 - d)}{md^0d} + \frac{M_2}{d} \qquad (2)$$

where M_2 is the molecular mass of $Y(NO_3)_3$, and ϕ_v is in units of cm³/mol. The ϕ_v values of $Y(NO_3)_3$ fall close to those of $Ho(NO_3)_3$ at all concentrations (*17*). In contrast ϕ_v values for YCl_3 fall between those of $TbCl_3$ and $DyCl_3$ (*19*). Ionic radius

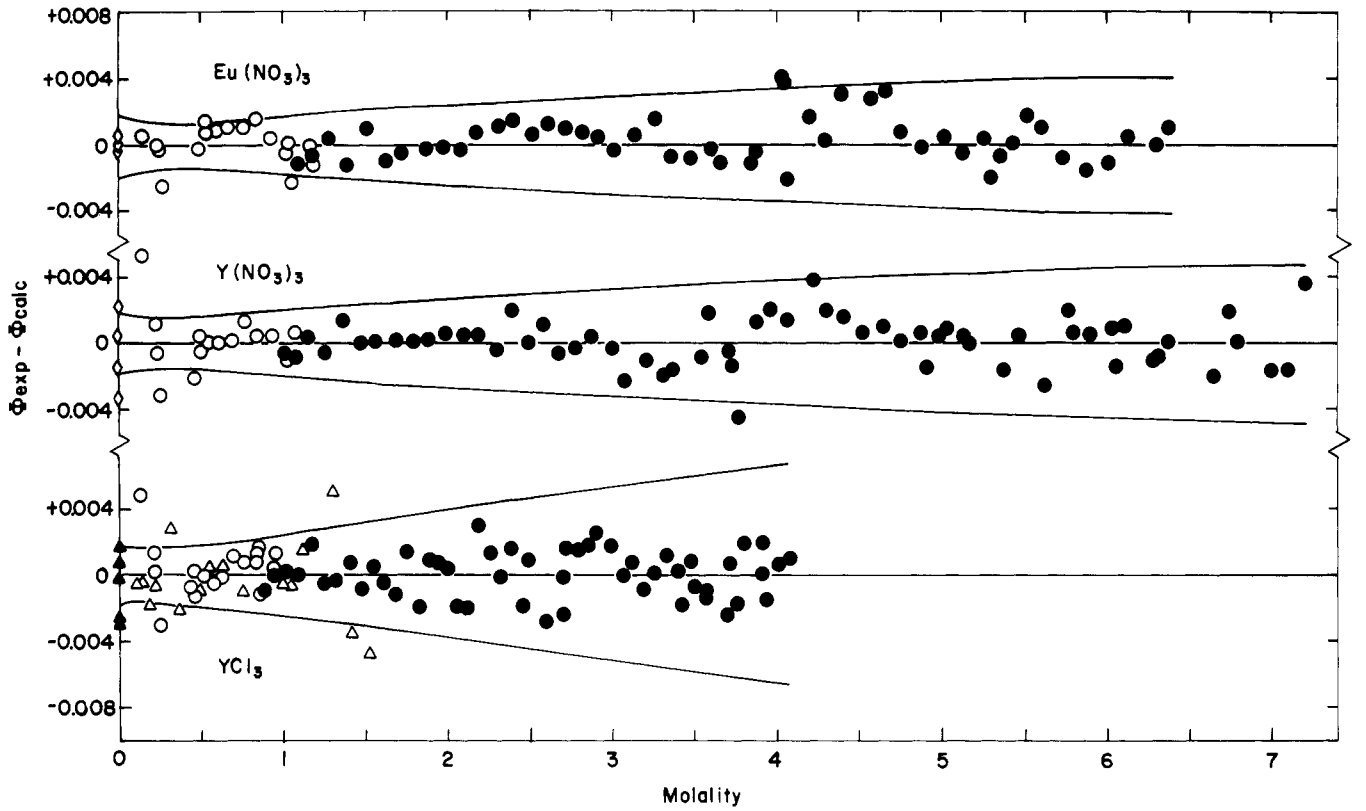

Figure 1. Differences between experimental and calculated osmotic coefficients of rare-earth electrolyte solutions at 25 °C: (●) this study, isopiestic vs. $CaCl_2$; (○) this study, isopiestic vs. KCl; (◇) estimated from electrical conductances; (▲) emf data; (△) Mason (*24*). Curves indicate deviations of ±0.2%.

considerations (*20*, *21*) would place Y^{3+} between Er^{3+} and Tm^{3+}.

The osmotic coefficients, Φ, of the rare-earth electrolyte solutions were calculated from the equation for isopiestic equilibrium

$$\Phi = \nu^* m^* \Phi^* / \nu m \tag{3}$$

where $\nu = 4$ is the number of ions formed by the complete dissociation of one molecule of rare-earth electrolyte, and m is the molal concentration. Asterisks indicate the corresponding quantities for the KCl or $CaCl_2$ isopiestic standards in equilibrium with rare-earth electrolyte solutions. Reference-solution Φ^* values were calculated by using available equations (*22*, *23*) and are reported in Tables I and II along with the isopiestic molalities.

Rare-earth electrolyte osmotic coefficients were represented by

$$\Phi = 1 - (A/3)m^{1/2} + \sum_i A_i m^{r_i} \tag{4}$$

where $A = 8.6430$ is the Debye–Hückel limiting slope for 3–1 electrolytes. Mean molal activity coefficients are then given by

$$\ln \gamma_\pm = -Am^{1/2} + \sum_i A_i \left(\frac{r_i + 1}{r_i}\right) m^{r_i} \tag{5}$$

Water activities can be calculated from

$$\ln a_1 = -\nu m M_1 \Phi / 1000 \tag{6}$$

where $M_1 = 18.0152$ g/mol is the molecular mass of water.

All of the osmotic coefficients of Tables I and II were given unit weights for least-squares fits with eq 4. Osmotic coefficients below 0.1 mol/kg are required to properly determine the coefficients of this equation. Dilute-solution Φ values are not available for $Eu(NO_3)_3$ or $Y(NO_3)_3$ so they were estimated (*5*) by using ion-size parameters derived from electrical conductance data. Dilute-solution Φ values for YCl_3 were interpolated from emf measurements for other rare-earth chlorides (*3*). These estimated Φ values were also given unit weights for the least-squares fits.

Other isopiestic data are available for YCl_3 solutions (*3*, *24*). Mason's data (*24*) (except for discrepant values at 0.071 and 0.135 mol/kg) were also included in the least-squares fits after recalculation to the standard Φ^* values used here (*22*). The data of Spedding et al. (*3*) are systematically low and were assigned zero weights. These rejected data are discrepant by as much as 1% at high concentrations. This is most probably due to a concentration analysis error in the earlier study.

Table V contains the parameters for the "best fits" to eq 4. Figure 1 illustrates the differences between the experimental Φ data and eq 4. Table VI contains calculated values of Φ, a_1, and $\gamma_\pm$ at various round concentrations.

Pitzer's equations (*25*, *26*) were also used to represent rare-earth nitrate Φ data to 2.0 mol/kg, and YCl_3 data to supersaturated concentrations. Parameters given in Table VII were computed by using Pitzer's recommended weighting scheme, with $3\beta^{(1)}/2 = 7.700$ for nitrates and 8.400 for chlorides (*25*). The Debye–Hückel slope A^ϕ was fixed at 0.3920.

Results and Discussion

Figure 2 illustrates the mean molal activity coefficients of rare-earth nitrate solutions, at constant molality, as a function of ionic radius (*20*, *21*). At low concentrations, $\gamma_\pm$ values decrease from $La(NO_3)_3$ to $Sm(NO_3)_3$ and then increase to $Lu(NO_3)_3$. By 1.0–1.2 mol/kg, $\gamma_\pm$ is nearly constant from $La(NO_3)_3$ to $Nd(NO_3)_3$ and then increases to $Lu(NO_3)_3$. At higher concentrations $\gamma_\pm$ increases from $La(NO_3)_3$ to $Lu(NO_3)_3$. Water activities (Figure 3) exhibit related trends but undergo a general decrease across the series.

Series trends for the rare-earth nitrates are easier to understand by comparison with those for the less complexed

Table VI. Osmotic Coefficients, Water Activities, and Activity Coefficients at Even Molalities

m, mol/kg	Φ	a_1	$\gamma_\pm$	m, mol/kg	Φ	a_1	$\gamma_\pm$
			$Eu(NO_3)_3$				
0.1	0.7417	0.994670	0.2960	3.0	1.4265	0.7346	0.4054
0.2	0.7435	0.98934	0.2478	3.2	1.4736	0.7119	0.4375
0.3	0.7566	0.98378	0.2267	3.4	1.5195	0.6892	0.4720
0.4	0.7737	0.97794	0.2156	3.6	1.5640	0.6665	0.5090
0.5	0.7932	0.97183	0.2094	3.8	1.6072	0.6440	0.5486
0.6	0.8143	0.96540	0.2063	4.0	1.6491	0.6217	0.5908
0.7	0.8367	0.95867	0.2054	4.2	1.6897	0.5997	0.6357
0.8	0.8601	0.95162	0.2060	4.4	1.7290	0.5780	0.6834
0.9	0.8844	0.94426	0.2079	4.6	1.7671	0.5567	0.7339
1.0	0.9093	0.93658	0.2109	4.8	1.8040	0.5358	0.7874
1.2	0.9606	0.92029	0.2193	5.0	1.8398	0.5154	0.8439
1.4	1.0133	0.90282	0.2307	5.2	1.8745	0.4954	0.9035
1.6	1.0666	0.8843	0.2446	5.4	1.9081	0.4759	0.9664
1.8	1.1201	0.8648	0.2609	5.6	1.9407	0.4570	1.033
2.0	1.1732	0.8444	0.2794	5.8	1.9724	0.4385	1.102
2.2	1.2258	0.8234	0.3001	6.0	2.0032	0.4206	1.175
2.4	1.2776	0.8018	0.3231	6.2	2.0331	0.4032	1.252
2.6	1.3284	0.7797	0.3482	6.3858	2.0602	0.3875	1.327
2.8	1.3780	0.7573	0.3757				
			$Y(NO_3)_3$				
0.1	0.7732	0.994443	0.3108	3.4	1.7202	0.6561	0.8526
0.2	0.7946	0.98861	0.2729	3.6	1.7666	0.6324	0.9319
0.3	0.8217	0.98239	0.2593	3.8	1.8117	0.6089	1.017
0.4	0.8505	0.97578	0.2545	4.0	1.8556	0.5857	1.109
0.5	0.8805	0.96877	0.2545	4.2	1.8982	0.5630	1.208
0.6	0.9113	0.96136	0.2575	4.4	1.9397	0.5406	1.314
0.7	0.9428	0.95356	0.2627	4.6	1.9801	0.5187	1.428
0.8	0.9747	0.94536	0.2698	4.8	2.0193	0.4973	1.550
0.9	1.0068	0.93679	0.2783	5.0	2.0575	0.4765	1.680
1.0	1.0391	0.92785	0.2881	5.2	2.0946	0.4562	1.819
1.2	1.1037	0.90897	0.3113	5.4	2.1306	0.4364	1.966
1.4	1.1676	0.8889	0.3388	5.6	2.1655	0.4173	2.123
1.6	1.2304	0.8677	0.3704	5.8	2.1992	0.3989	2.289
1.8	1.2917	0.8457	0.4061	6.0	2.2317	0.3810	2.464
2.0	1.3513	0.8230	0.4459	6.2	2.2629	0.3638	2.648
2.2	1.4092	0.7998	0.4899	6.4	2.2927	0.3474	2.841
2.4	1.4652	0.7761	0.5382	6.6	2.3211	0.3316	3.043
2.6	1.5195	0.7522	0.5911	6.8	2.3480	0.3165	3.253
2.8	1.5721	0.7282	0.6487	7.0	2.3732	0.3021	3.470
3.0	1.6230	0.7041	0.7113	7.2	2.3965	0.2884	3.693
3.2	1.6724	0.6800	0.7792	7.2103	2.3977	0.2877	3.705
			YCl_3				
0.1	0.7829	0.994374	0.3401	2.0	1.9444	0.7556	1.248
0.2	0.8100	0.98840	0.3027	2.2	2.0948	0.7174	1.599
0.3	0.8490	0.98181	0.2935	2.4	2.2426	0.6785	2.052
0.4	0.8926	0.97460	0.2953	2.6	2.3864	0.6395	2.632
0.5	0.9396	0.96671	0.3037	2.8	2.5254	0.6008	3.369
0.6	0.9897	0.95811	0.3172	3.0	2.6590	0.5628	4.297
0.7	1.0430	0.94875	0.3353	3.2	2.7871	0.5259	5.459
0.8	1.0994	0.93859	0.3582	3.4	2.9102	0.4902	6.906
0.9	1.1590	0.92759	0.3859	3.6	3.0288	0.4558	8.701
1.0	1.2215	0.91574	0.4191	3.8	3.1440	0.4228	10.93
1.2	1.3542	0.8895	0.5041	3.9367[a]	3.2215	0.4010	12.76
1.4	1.4954	0.8600	0.6196	4.0	3.2572	0.3911	13.70
1.6	1.6424	0.8275	0.7742	4.0843	3.3048	0.3781	15.07
1.8	1.7929	0.7925	0.9791				

[a] Saturated solution.

Table VII. Parameters for Pitzer's Equations

parameter	$Eu(NO_3)_3$	$Y(NO_3)_3$	YCl_3
$3\beta^{(0)}/2$	0.7133	0.9158	0.9396
$3\beta^{(1)}/2$	7.700	7.700	8.400
$(3^{3/2}/2)C^{\Phi}$	−0.1257	−0.1898	−0.0406
σ	0.0068	0.0085	0.0060

rare-earth chloride and perchlorate solutions (*3*, *4*). Figures 4 and 5 show ln $\gamma_\pm$ and a_1 for these three series at 2.0 mol/kg. The a_1 values show a general decrease, and $\gamma_\pm$ an increase, from La^{3+} to Lu^{3+} for all three anions. At a given low or moderate concentration the chloride and perchlorate ln $\gamma_\pm$ and a_1 values are S-shaped, whereas the nitrates have extrema at $Sm(NO_3)_3$ for concentrations below 1.0 mol/kg.

The ionic radius of a rare-earth ion decreases from La^{3+} to Lu^{3+} (lanthanide contraction). This decreasing ionic radius causes an increase in the electrical charge density at the surface of the ion, and thereby an increase in ion-dipole forces between the rare-earth ion and water. The net result is that total ionic hydration increases with the decrease in ionic radius. In addition, an inner-sphere hydration number decrease is believed to occur between Nd^{3+} and Tb^{3+} resulting from the decreasing ionic size (*8*). The radius of the inner hydration sphere shrinks more rapidly with bare-ion radius when this inner-sphere hydration change occurs, since fewer waters occupy the inner sphere. This inner-sphere hydrated radius decrease shows up clearly in X-ray diffraction data (*9*).

As the inner hydration sphere radius decreases, water

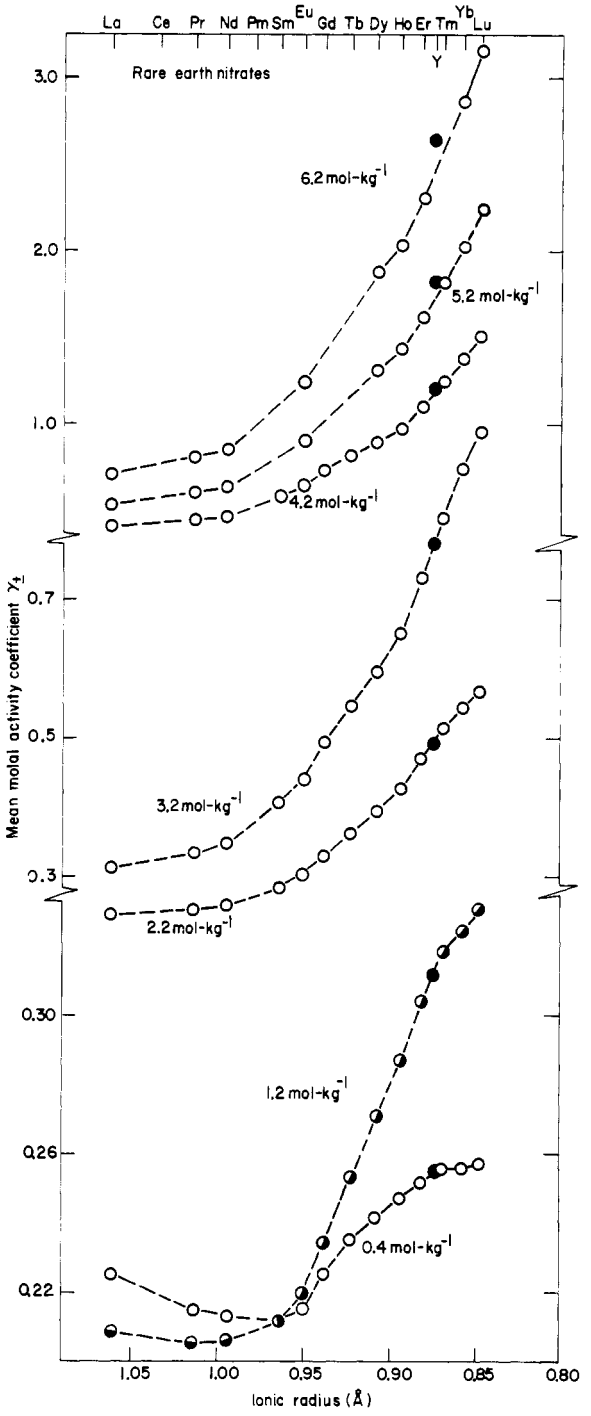

Figure 2. Mean molal activity coefficients of rare-earth nitrate solutions at constant molalities. Filled circles indicate $Y(NO_3)_3$.

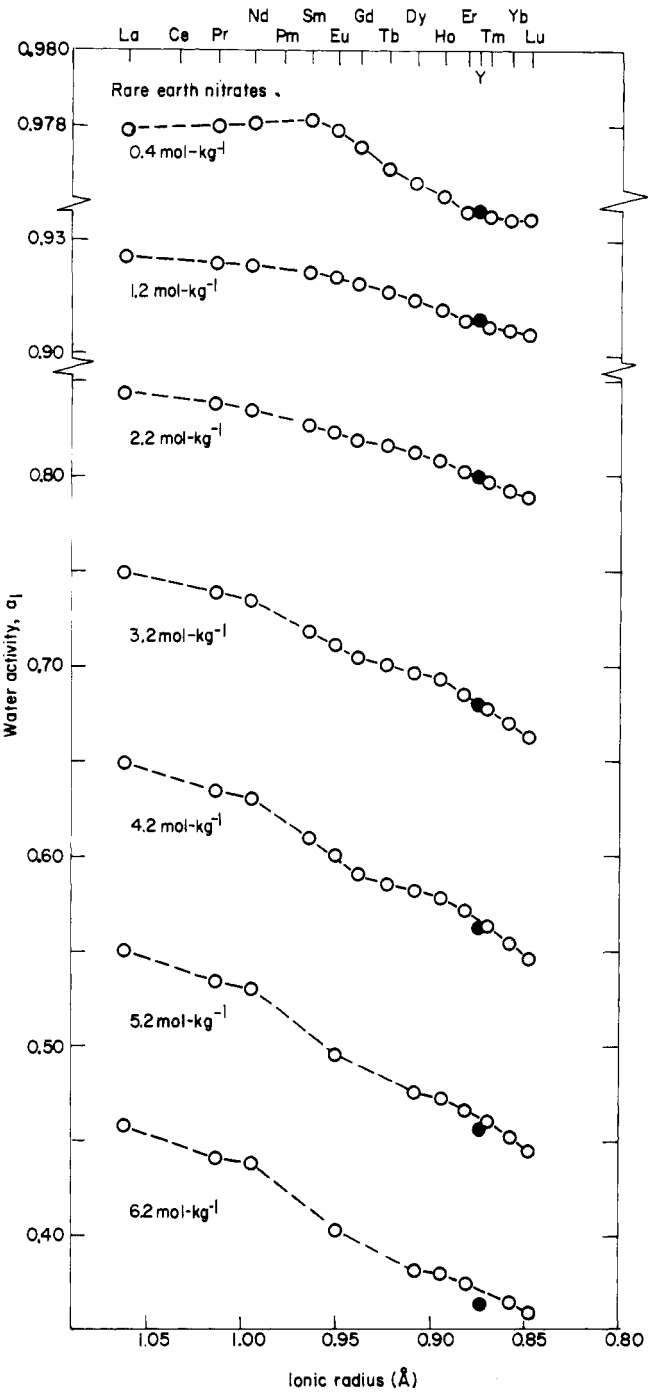

Figure 3. Water activities of rare-earth nitrate solutions at constant molalities. Filled circles indicate $Y(NO_3)_3$.

molecules in the second sphere and further out move in more closely so total hydration increases from La^{3+} to Lu^{3+}, with the most rapid change being between Nd^{3+} and Tb^{3+}. Water activities are intimately related to ionic hydration, so a_1 values have S-shaped trends (Figure 5) with decreases from La^{3+} to Lu^{3+}. Standard-state ionic entropies (*27*) and ionic Jones–Dole viscosity *B* coefficients (*28*) can also be explained by this same model. Lugina and Davidenko (*29*) have found that rare-earth perchlorates also undergo solvation changes with Me_2SO in nitromethane.

This model should apply if complex formation between anion and cation is weak and series trends are dominated by cation hydration. Available evidence indicates that rare-earth chlorides and perchlorates only form weak outer-sphere ion pairs (*30–35*) so the model applies to them. This increase in total hydration with decrease in ionic radius should break down at high concentrations since there will not be enough water to separately satisfy all of the hydration requirements of the individual ions. Since the strength and extent of solvent sharing should increase with decreasing bare-ion radius (increasing charge density), a_1 still decreases from La^{3+} to Lu^{3+}. Although the trend in a_1 is no longer strictly S-shaped, there is a displacement of Sm^{3+}–Lu^{3+} from the La^{3+}–Nd^{3+} trend which is caused by the inner-sphere hydration number decrease.

The rare-earth nitrates show considerably different series trends, which seem to be due to stronger and more extensive complex formation. The rare-earth nitrate a_1 values are higher, and $\gamma_\pm$ values lower, than for the chlorides and perchlorates. This is expected since complex formation reduces the number of free ions and displaces tightly bound water from the cation hydration sheath.

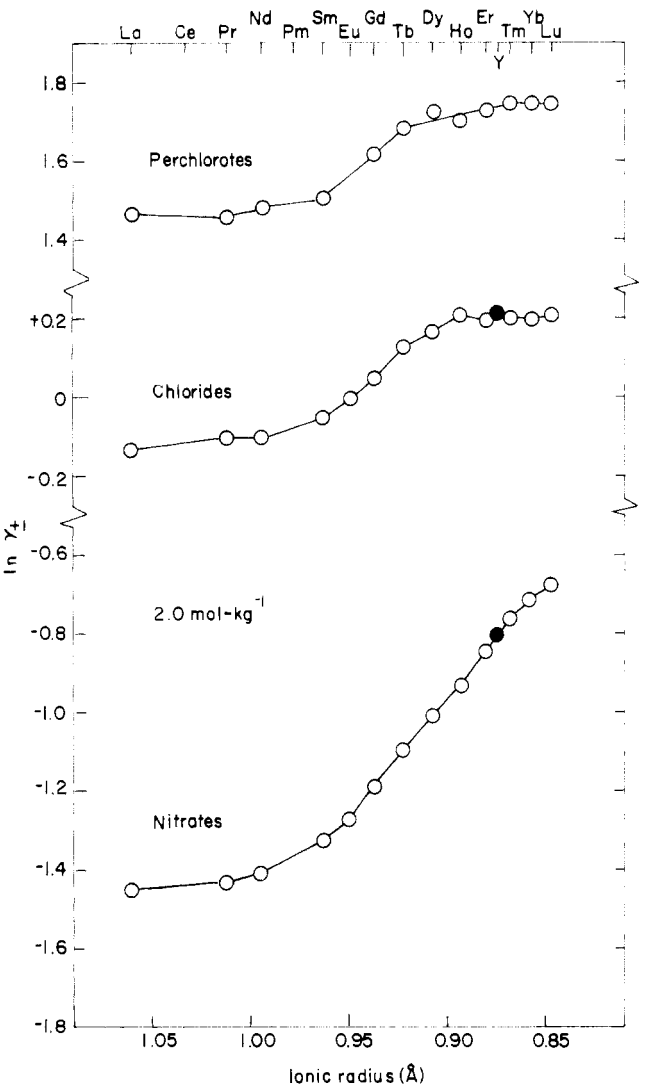

Figure 4. Natural logarithms of the mean molal activity coefficients of rare-earth electrolyte solutions at 2.0 mol/kg. Filled circles indicate Y^{3+} salts.

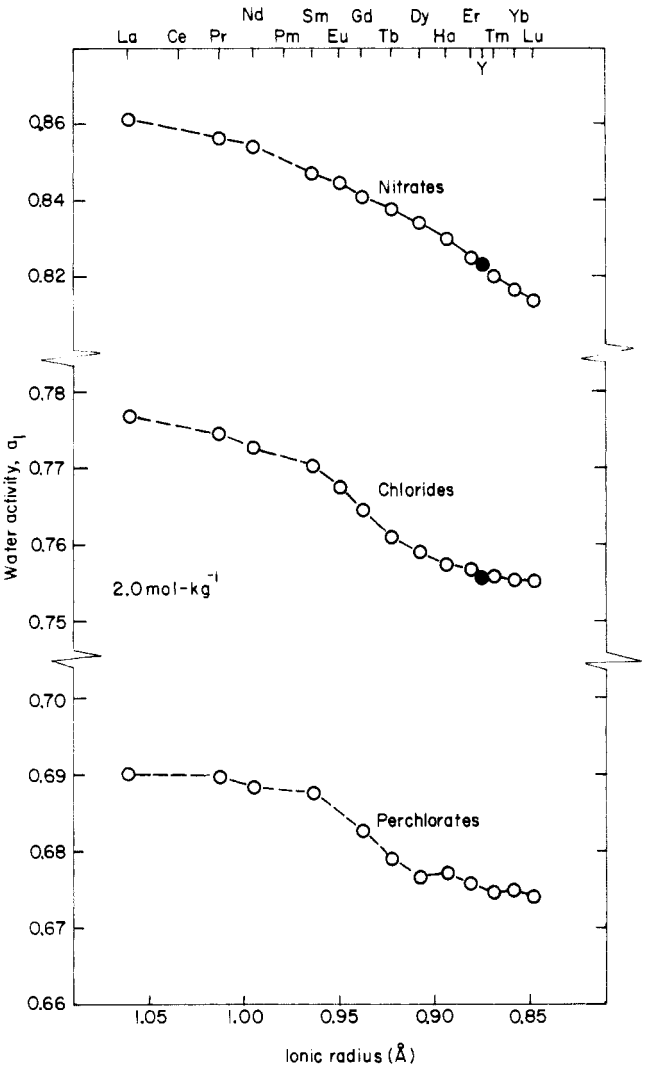

Figure 5. Water activities of rare-earth electrolyte solutions at 2.0 mol/kg. Filled circles indicate Y^{3+} salts.

Marcantonatos et al. (*36*) have suggested that $Eu(NO_3)_3$ contains no inner-sphere nitrate complexes in the Eu^{3+} ground state (but they form in the $^5D_0$ state). In contrast, Choppin et al. (*31*) felt that visible and IR spectra indicated a mixture of inner- and outer-sphere complexes, with most being outer-sphere. However, a number of other properties show sizable shifts with the addition of nitrate ions, and this indicates that a significant fraction of inner-sphere complexes are present. These properties include NMR (*32*, *37*, *38*), molar absorptivity (*37*), and ultrasonic absorption (*39*, *40*). Also, $Eu(NO_3)_3$ fluorescence spectra (*41*) indicate that above 0.01 mol/dm^3 Eu^{3+} has a symmetry different from the aquo ion.

Trends in the series behavior of $\gamma_\pm$ and a_1 of rare-earth nitrates (Figures 2 and 3) allow one to reach conclusions about the variation of the extent of complex formation with ionic radius. Figure 2 indicates that $\gamma_\pm$ has a minimum at $Sm(NO_3)_3$ at low concentrations; however, no minimum is present for chlorides and perchlorates. This implies that the amount of complex formation increases from $La(NO_3)_3$ to $Sm(NO_3)_3$ and then decreases to $Lu(NO_3)_3$. Published stability constant data are consistent with this conclusion (*42*, *43*). Above 1.0–1.2 mol/kg $\gamma_\pm$ increases from $La(NO_3)_3$ to $Lu(NO_3)_3$; this implies that complex formation decreases from $La(NO_3)_3$ to $Lu(NO_3)_3$ at high concentrations. Electrical conductance data for rare-earth nitrate solutions show the same trends as $\gamma_\pm$, with the minimum disappearing at about 0.9 mol/kg (*44*).

There is a "bulge" present in the rare-earth nitrate $\gamma_\pm$ and a_1 curves at high concentrations, with the tip of this bulge occurring at $Gd(NO_3)_3$. This indicates that a Gd break is present for the solution excess free energies. However, this anomaly is small relative to series trends and could be due to causes other than the added stability of a half-filled 4f orbital (such as size or shape factors).

Values of a_1 and $\gamma_\pm$ for $Y(NO_3)_3$ indicate that it behaves as expected for its ionic radius up to about 3.2 mol/kg. At higher concentrations $Y(NO_3)_3$ activities shift relative to the other rare-earth nitrates. The a_1 values even cross the $Lu(NO_3)_3$ curve by 7.04 mol/kg. This indicates that lower-order complexes in $Y(NO_3)_3$ solutions are comparable in strength to other rare-earth nitrates with similar cation radius. However, higher-order complexes of $Y(NO_3)_3$ are probably less stable than for all other rare-earth nitrates since a_1 becomes lowest for $Y(NO_3)_3$ at high concentrations.

Our study of rare-earth activity data is now complete.

Acknowledgment

We thank Donald G. Miller (LLNL) for help with calculations and for suggestions to improve this manuscript and Sandy Auguadro (LLNL Correspondence Center, A.D. Administrative) for her skilled word-processing/typing of this manuscript.

Glossary

d	density of solution, g/cm^3
d^0	density of pure water, g/cm^3
ϕ_v	apparent molal volume, cm^3/mol
Φ	molal osmotic coefficient
ν	number of ions formed by the dissociation of one molecule of solute
m	molal concentration of the solute, mol/kg
c	molar concentration of the solute, mol/dm^3
*	symbols with asterisks refer to KCl or $CaCl_2$ isopiestic standards
B_l	least-squares coefficients of eq 1
A_l	least-squares coefficients of eq 4 and 5
r_l	powers of eq 4 and 5
A	Debye–Hückel constant for 3–1 electrolytes
M_1	molecular mass of water, g/mol
M_2	molecular mass of solute, g/mol
$\beta^{(0)}$, $\beta^{(1)}$, C^ϕ	parameters for Pitzer's equations
A^ϕ	Debye–Hückel constant for Pitzer's Φ equations (1–1 charge type)
σ	standard deviation of fitting equations
$\gamma_\pm$	mean molal activity coefficient
a_1	water activity

Literature Cited

(1) Spedding, F. H.; Atkinson, G. In "The Structure of Electrolytic Solutions"; Hamer, W. J., Ed.; Wiley: New York, 1959.
(2) Spedding, F. H.; Nelson, R. A.; Rard, J. A. *J. Chem. Eng. Data* **1974**, *19*, 379.
(3) Spedding, F. H.; Weber, H. O.; Saeger, V. W.; Petheram, H. H.; Rard, J. A.; Habenschuss, A. *J. Chem. Eng. Data* **1976**, *21*, 341.
(4) Rard, J. A.; Weber, H. O.; Spedding, F. H. *J. Chem. Eng. Data* **1977**, *22*, 187.
(5) Rard, J. A.; Shiers, L. E.; Heiser, D. J.; Spedding, F. H. *J. Chem. Eng. Data* **1977**, *22*, 337.
(6) Rard, J. A.; Miller, D. G.; Spedding, F. H. *J. Chem. Eng. Data* **1979**, *24*, 348.
(7) Rard, J. A.; Spedding, F. H. *J. Chem. Eng. Data* **1981**, *26*, 391.
(8) Spedding, F. H.; Pikal, M. J.; Ayers, B. O. *J. Phys. Chem.* **1966**, *70*, 2440.
(9) Habenschuss, A.; Spedding, F. H. *J. Chem. Phys.* **1980**, *73*, 442.
(10) Spedding, F. H.; DeKock, C. W.; Pepple, G. W.; Habenschuss, A. *J. Chem. Eng. Data* **1977**, *22*, 58.
(11) Spedding, F. H.; Baker, J. L.; Walters, J. P. *J. Chem. Eng. Data* **1975**, *20*, 189.
(12) Spedding, F. H.; Rard, J. A. *J. Phys. Chem.* **1974**, *78*, 1435.
(13) Spedding, F. H.; Witte, D. L.; Shiers, L. E.; Rard, J. A. *J. Chem. Eng. Data* **1974**, *19*, 369.
(14) Rard, J. A.; Miller, D. G. *J. Chem. Eng. Data* **1981**, *26*, 38.
(15) West, P. W.; Sarma, P. L. *Mikrochimica Acta* **1957**, 506.
(16) Duval, C. "Inorganic Thermogravimetric Analysis", 2nd ed. revised (English Translation); Elsevier: Amsterdam, 1963.
(17) Spedding, F. H.; Shiers, L. E.; Brown, M. A.; Baker, J. L.; Gutierrez, L.; McDowell, L. S.; Habenschuss, A. *J. Phys. Chem.* **1975**, *79*, 1087.
(18) Kell, G. S. *J. Chem. Eng. Data* **1975**, *20*, 97.
(19) Spedding, F. H.; Saeger, V. W.; Gray, K. A.; Boneau, P. K.; Brown, M. A.; DeKock, C. W.; Baker, J. L.; Shiers, L. E.; Weber, H. O.; Habenschuss, A. *J. Chem. Eng. Data* **1975**, *20*, 72.
(20) Templeton, D. H.; Dauben, C. H. *J. Am. Chem. Soc.* **1954**, *76*, 5237.
(21) Zachariasen, W. H. In "The Actinide Elements"; Seaborg, G. T., Katz, J. J., Eds.; McGraw-Hill: New York, 1954; Chapter 18.
(22) Hamer, W. J.; Wu, Y. C. *J. Phys. Chem. Ref. Data* **1972**, *1*, 1047.
(23) Rard, J. A.; Habenschuss, A.; Spedding, F. H. *J. Chem. Eng. Data* **1977**, *22*, 180.
(24) Mason, C. M. *J. Am. Chem. Soc.* **1938**, *60*, 1638.
(25) Pitzer, K. S.; Peterson, J. R.; Silvester, L. F. *J. Solution Chem.* **1978**, *7*, 45.
(26) Pitzer, K. S. In "Activity Coefficients in Electrolyte Solutions"; Pytkowicz, R. M., Ed.; CRC Press: Boca Raton, FL, 1979; Vol. 1, Chapter 7.
(27) Spedding, F. H.; Rard, J. A.; Habenschuss, A. *J. Phys. Chem.* **1977**, *81*, 1069.
(28) Spedding, F. H.; Shiers, L. E.; Rard, J. A. *J. Chem. Eng. Data* **1975**, *20*, 66.
(29) Lugina, L. N.; Davidenko, N. K. *Russ. J. Inorg. Chem.* (*Engl. Trans.*) **1980**, *25*, 1322.
(30) Sayre, E. V.; Miller, D. G.; Freed, S. *J. Chem. Phys.* **1957**, *26*, 109.
(31) Choppin, G. R.; Henrie, D. E.; Buijs, K. *Inorg. Chem.* **1966**, *5*, 1743.
(32) Reuben, J.; Fiat, D. *J. Chem. Phys.* **1969**, *51*, 4909.
(33) Marcinkowsky, A. E.; Phillips, H. O. *J. Chem. Soc. A* **1971**, 3556.
(34) Kozachenko, N. N.; Batyaev, I. M. *Russ. J. Inorg. Chem.* (*Engl. Trans.*) **1971**, *16*, 66.
(35) Bünzli, J.-C. G.; Yersin, J.-R. *Inorg. Chem.* **1979**, *18*, 605.
(36) Marcantonatos, M. D.; Deschaux, M.; Vuilleumier, J. J. *Chem. Phys. Lett.* **1981**, *82*, 36.
(37) Abrahamer, I.; Marcus, Y. *Inorg.* Chem. **1987**, *6*, 2103.
(38) Reuben, J. *J. Phys. Chem.* **1975**, *79*, 2154.
(39) Silber, H. B.; Fowler, J. *J. Phys. Chem.* **1976**, *80*, 1451.
(40) Jezowska-Trzebiatowska, B.; Ernst, S.; Legendziewicz, J.; Oczko, G. *Bull. Acad. Pol. Sci., Ser. Sci. Chim.* **1977**, *25*, 649.
(41) Freed, S.; Jacobson, H. F. *J. Chem. Phys.* **1938**, *6*, 654.
(42) Choppin, G. R.; Strazik, W. F. *Inorg. Chem.* **1965**, *4*, 1250.
(43) Peppard, D. F.; Mason, G. W.; Hucher, I. *J. Inorg. Nucl. Chem.* **1962**, *24*, 881.
(44) Rard, J. A.; Spedding, F. H. *J. Phys. Chem.* **1975**, *79*, 257.

Received for review April 8, 1982. Accepted June 7, 1982. This work was performed under the auspices of the Office of Basic Energy Science of the U.S. Department of Energy by Lawrence Livermore National Laboratory under contract No. W-7405-ENG-48.

Solubility of Hydrogen in *o*-Nitroanisole, *o*-Nitroanisole–Methanol Mixtures, and *o*-Anisidine†

Prabhakar H. Brahme,* Hemant G. Vadgaonkar, Prakash S. Ozarde, and Madan G. Parande

National Chemical Laboratory, Poona 411 008, India

The solubility of hydrogen in *o*-nitroanisole, *o*-nitroanisole–methanol mixtures, and *o*-anisidine is determined at temperatures between 40 and 80 °C and pressures between 7 and 50 atm. The values of Henry's law constant and heat of solution are reported.

A precise knowledge of solubility of gases in liquids is essential for analyzing gas–liquid and gas–liquid–solid reactions. This paper presents solubility data of hydrogen in *o*-nitroanisole, *o*-nitroanisole–methanol mixtures, and *o*-anisidine under various conditions of temperature and pressure. The data are important in the design of a reactor for *o*-anisidine which is manufactured by catalytic hydrogenation of *o*-nitroanisole. No data have been published for the solubility of hydrogen in *o*-nitroanisole and *o*-anisidine. The solubility of hydrogen in *o*-nitroanisole, *o*-nitroanisole–methanol mixtures, and *o*-anisidine was studied in the range of interest for hydrogenation, namely, 40–80 °C, 7–50 atm, and 3–8 M concentration.

Commercially available *o*-nitroanisole and *o*-nitroanisidine of

† NCL Communication No. 2976.

0021-9568/82/1727-0461$01.25/0